The Triple Spar Campaign: Implementation and Test of a Blade Pitch Controller on a Scaled Floating Wind Turbine Model

Yu, Wenye; Lemmer, F.; Bredmose, Henrik; Borg, Michael; Pegalajar Jurado, Antonio Manuel; Mikkelsen, Robert Flemming; Larsen, T. Stoklund; Fjelstrup, T.; Lomholt, Anders Kjær; Boehm, L.

Total number of authors:
13

Published in:
Energy Procedia

Link to article, DOI:
10.1016/j.egypro.2017.10.357

Publication date:
2017

Document Version
Publisher's PDF, also known as Version of record

Available online at www.sciencedirect.com

ScienceDirect

Energy Procedia 137 (2017) 323–338

Energy Procedia

www.elsevier.com/locate/procedia

14th Deep Sea Offshore Wind R&D Conference, EERA DeepWind'2017, 18-20 January 2017, Trondheim, Norway

The Triple Spar Campaign: Implementation and Test of a Blade Pitch Controller on a Scaled Floating Wind Turbine Model

W. Yu[a,*], F. Lemmer[a], H. Bredmose[b], M. Borg[b], A. Pegalajar-Jurado[b], R. F. Mikkelsen[b], T. Stoklund Larsen[b], T. Fjelstrup[b], A. K. Lomholt[b], L. Boehm[b], D. Schlipf[a], J. Azcona Armendariz[c], P. W. Cheng[a]

[a]*Stuttgart Wind Energy, University of Stuttgart, Allmandring 5B, 70569 Stuttgart, Germany*
[b]*DTU Wind Energy, Nils Koppels Allé Building 403, DK-2800 Kgs. Lyngby, Denmark*
[c]*CENER, Ciudad de la Innovacion, no. 7, 31621 Sarriguren (Navarra), Spain*

Abstract

In this project by the University of Stuttgart, DTU Wind Energy and CENER, a real-time blade-pitch control system was implemented on a scaled model in a combined wind-and-wave tank. A simplified low-order simulation model including aerodynamics, hydrodynamics, mooring dynamics and structural dynamics was used to design the controller. Some effort has been made to investigate the influence of different gain scheduling methodologies of the collective blade-pitch controller on the dynamic behavior of the floating wind turbine. The issue relating to the negative aerodynamic damping is also investigated in order to find out whether the effects seen in simulation models can be equally reproduced by model tests. Additionally, wind and wave-induced responses with different gain scheduling methodologies and the difference to the tests without blade-pitch control are discussed. A solution for the hardware implementation of the real-time controller has been introduced. The developed controller is proven to function throughout the test campaign, which also proves the reliability of the simplified simulation model for controller design. It has been shown that with the low-Reynolds rotor it is possible to control the rotor speed at Froude-scaled frequencies by actuating the blade pitch angle.

Peer-review under responsibility of SINTEF Energi AS.

* Wei Yu. Tel.: +49-711-685-68240; fax: +49-711-685-68293.
E-mail address: yu@ifb.uni-stuttgart.de

1876-6102
Peer-review under responsibility of SINTEF Energi AS.
10.1016/j.egypro.2017.10.357

Keywords: Floating wind turbine; scaled model test; controller design; controller implementation

1. Introduction

The wind and wave induced response of floating offshore wind turbines (FOWT) is rather complex and reflects the rotor aerodynamics, tower elasticity, blade-pitch control, incident waves, floating platform dynamic properties, and the mooring dynamics. Theoretical developments, simulation models and validation data are needed to understand these coupled dynamics. Several coupled aero-hydro-servo-elastic codes have already been developed for the analysis and design of FOWTs. The verification of these codes by direct code-to-code comparison through the Offshore Code Comparison Collaboration (OC3) and the Offshore Code Comparison Collaboration Continuation (OC4) projects had a benchmarking success. A significant number of model tests for FOWTs have also been performed to validate the simulation codes. One open question of these model tests is the scaling methodology of the aerodynamic forces. As a solution discussed in [1], newly designed blades, which yield the correctly (Froude-) scaled thrust force, are mostly used for combined wind-and-wave model tests of FOWT. The Froude-scaled model requires re-designing the blades for low Reynolds numbers, which implies that the aerodynamic torque is not correctly scaled and the control system should be redesigned. Due to the complexity, in the past tests as for full-scale turbines, blade-pitch control has not been included but the rotor speed was kept constant through a servomotor. Recent research has investigated the so-called instability problem in the platform-pitch mode because of the negative aerodynamic damping, which is due to the significantly reduced frequency of the tower-top displacement mode. Several solutions have been introduced and verified with simulations, through which the effect of the controller on the dynamic response of FOWTs has been indicated. To take this into account, a combined wind-and-wave model test with fixed blade-pitch and constant rotor speed is not sufficient. One method to include the aerodynamic damping is the Software-in-the-Loop method, which is based on the use of a ducted fan substituting the wind turbine scaled rotor [2]. The fan yields a realistic force to represent the aerodynamic thrust through the fan rotational speed governed by a controller. However, the inertial properties of the rotor are not represented correctly, which change the natural frequencies and the modes shapes of the tower. The motivation of this paper is to demonstrate a solution to include the aerodynamic damping, introducing the controller design and implementation for FOWT model tests. For this, the controller is not scaled-down from the full-scale model but re-designed for the scaled model and the low-Reynolds airfoils. The paper describes first the simulation model and the controller design procedure and finally a comparison of the numerical and experimental responses with a discussion.

2. Simulation model

The simplified simulation model used for the design of the controllers in the experimental tests is briefly described in this section. It was also calibrated through several identification tests.

2.1. Reduced simulation model

Figure 1 presents the 1:60 scaled DTU 10MW reference wind turbine (RWT) test model [3], which is mounted on a generic concrete floating platform model. The platform concept Triple Spar is a hybrid between a spar and a semi-submersible, developed originally in the project INNWIND.EU (see [4]) and was built at the University of Stuttgart. The wind turbine model, which represents the DTU 10 MW RWT, is constructed at the Danish Technical University (DTU). The rotor blades have low-Reynolds-number airfoils to produce the Froude-scaled thrust force. An overview of the campaign will be shown in the companion paper [5]. The rated wind speed of the scaled model is defined at $1.47\ \mathrm{m/s}$ and rotor speed at $71\ \mathrm{rpm}$.

A simulation model is needed to design a controller specifically for the scaled model. Thus, prior to the tests at DHI/Denmark, a simplified low-order simulation model was set up with only 3 rigid bodies: platform, tower, nacelle and a total of 5 degrees of freedom (DOFs): surge, heave, pitch, tower top displacement in downwind direction and the azimuth of the rotor. The joints and the DOFs are marked with red color in the sketch in Figure 1 (b). A fixed coordinate system with its origin on the sea water level and at the initial center of flotation is used to describe the

platform's position and orientation, which is also presented in Figure 1 (b). BEM theory is used to obtain the aerodynamic coefficients of the rotor. Frequency dependent linear hydrodynamic coefficients, e.g. first order hydrodynamic radiation (added mass, radiation damping) and diffraction forces are calculated with ANSYS-AQWA and then scaled to the model size according to the Froude similarity, which is the common procedure in offshore engineering. The added mass is also calibrated later in a preceding free-decay test. The mooring dynamics are solved using a quasi-static nonlinear model. The simulation models were augmented with the discrete-time properties of the selected hardware and the noise properties of the sensors in the experiment in order to realistically simulate the model beforehand.

a b

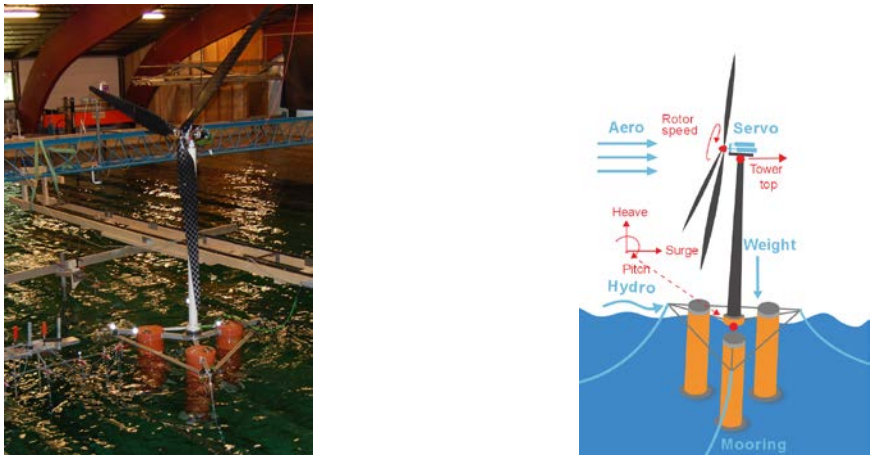

Figure 1: (a) Test model setup; (b) Simulation model and coordinate system.

2.2. Calibration of simulation model

A Froude-scaled rotor with low-Reynolds airfoils is designed to match only the thrust, which means that the aerodynamic power cannot be scaled with the Froude scaling law. This is due to the difficulty in calculating the lift and drag coefficients at relatively low Reynolds numbers. A high uncertainty is associated with aerodynamic losses and the drivetrain mechanical friction et cetera, and therefore a calibration with experimental measurements is necessary. Thus, the aerodynamic power coefficient c_P is firstly analyzed with the BEM method and then calibrated through a rotor-identification test with a clamped tower base, the test setup of which is presented in Figure 2. The power coefficient was measured at several operation points with different combinations of blade-pitch angle and tip speed ratio. The measurements were compared to a simulation model with a BEM-model, whose result is presented in Figure 3. As aerodynamic losses are significantly increased through the low Reynolds numbers it was as expected that the simulation model power coefficient differs from the test, depicted through yellow lines in Figure 3. To calibrate the aerodynamic model with less complexity, a total loss efficiency factor of 65% was chosen by minimizing the total deviation between the results of the simulation and the test, which can be seen in Figure 3. As a result, this factor was added to the BEM simulation model, which was used for the controller design.

Figure 2: Setup of bottom fixed rotor identification test.

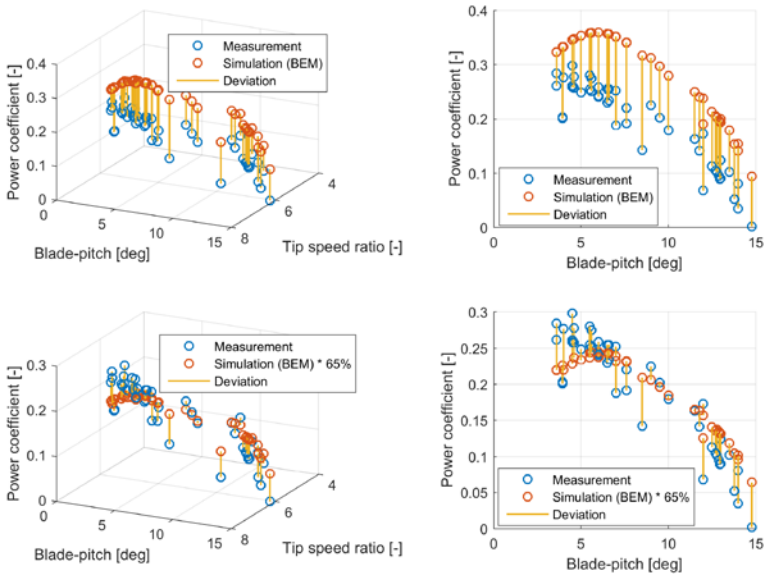

Figure 3: Calibration of aerodynamic power coefficient.

Since potential flow theory neglects the viscosity of water and hence does not consider non-linear viscous damping, the hydrodynamics were calibrated with free decay tests in surge, heave and pitch directions. As an example, pitch decay is shown in Figure 4. The natural frequency was estimated and the damping ratio was calculated by fitting the envelope line of the amplitudes. The non-linear viscous damping was simplified as a linear damping and then added to the simulation model. To verify the calibration, free decay tests were simulated and compared to the tests. Figure 4 (b) shows a good match for the pitch decay test.

a b

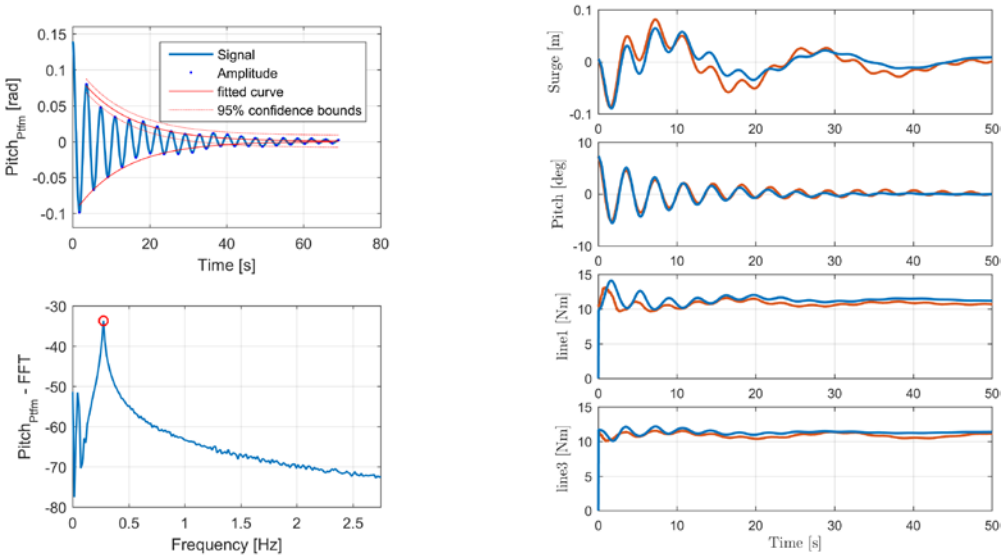

Figure 4: (a) Free decay test in time and frequency domain; (b) Result of hydrodynamic calibration.

3. Controller design

Two different methods of controller design are used for the blade-pitch controller for the model test; one is based on the NREL 5MW baseline controller and detuned according to [6] and [7], and the other is based on a coupling design method which is presented in [8].

3.1. Principle concept of the pitch controller

The controller for the scaled test model is based on the NREL 5MW baseline controller [9], which is a gain-scheduled proportional-integral (PI) controller. The objective is to obtain the optimal tip speed ratio by regulating the generate torque under rated wind speed and keep a stable rotor speed by blade-pitching above rated. A servomotor produces the generator torque. Regardless of the 1:5 gear ratio, the following discussion only uses the corresponding rotor speed (low speed shaft) to avoid confusion.

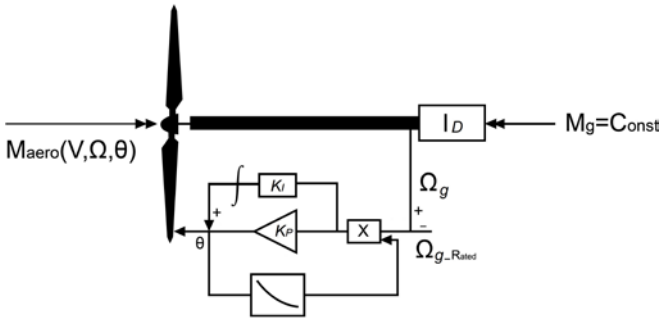

Figure 5: Blade-pitch control block diagram.

The torque controller below the rated wind speed is implemented in the same way as the baseline controller to ensure the safe transition between under-rated and above-rated wind speeds, although the focus of the tests is above-

rated conditions. The principle concept of the pitch controller is described in Figure 5. When only 1-DOF is considered, i.e. the drivetrain rotational speed, the nonlinear equation of the wind turbine drivetrain motion is:

$$I_D\ddot{\varphi} = M_a(V, \Omega, \theta) - M_g\,, \tag{1}$$

where I_D is the inertia of the isolated drivetrain, φ is the angular position of the servo motor, M_a and M_g are aerodynamic torque and motor torque, and V, Ω and θ are wind speed, rotor speed and blade-pitch angle, respectively. At a steady operating point, the aerodynamic torque equals the motor torque, such that the rotor speed is kept constant, i.e. $I_D\ddot{\varphi} = 0$. In the region above rated wind speed, when the generator torque is usually kept constant and there is a disturbance from the wind, the motor speed will change due to the change of aerodynamic torque. For a negligible fluctuation of the rotor speed and the incoming wind speed, the aerodynamic torque can be linearized as:

$$M_a(V, \Omega, \theta) = M_{a,0} + \left(\frac{\delta M_a}{\delta \theta}\right)\Delta\theta. \tag{2}$$

Considering that $M_{a,0} = M_{g,0}$, the equation of the drivetrain motion is:

$$I_D\ddot{\varphi} = \left(\frac{\delta M_a}{\delta \theta}\right)\Delta\theta. \tag{3}$$

The blade-pitch controller feeds back the speed error to the pitch angle

$$\Delta\theta = K_P\Delta\Omega_g + K_I\int_0^t \Delta\Omega_g dt = K_P\dot{\varphi} + K_I\varphi\,, \tag{4}$$

where K_P and K_I denote the coefficients of the proportional and integral terms respectively. Finally, the linear closed-loop equation, valid around the operating point can be represented as:

$$I_D\ddot{\varphi} + \left(-\frac{\delta M_a}{\delta \theta}\right)K_P\dot{\varphi} + \left(-\frac{\delta M_a}{\delta \theta}\right)K_I\varphi = 0, \tag{5}$$

which has the form of an ordinary second-order system, where the natural frequency ω_Ω and the damping ratio ζ_Ω depends on the controller parameters

$$\begin{aligned} \omega_\Omega^2 &= \left(-\frac{\delta M_a}{\delta \theta}\right)K_I\frac{1}{I_D}, \\ 2\omega_\Omega\zeta_\Omega &= \left(-\frac{\delta M_a}{\delta \theta}\right)K_P\frac{1}{I_D}. \end{aligned} \tag{6}$$

3.2. Negative aerodynamic damping

Earlier work [6] has shown the potential instability of the platform-pitch mode of FOWTs with a conventional land-based pitch controller. This results from the aerodynamic negative damping, when the natural frequency of the drivetrain closed-loop is higher than the natural frequency of the platform pitch mode. The reason can be described with the equation of platform-pitch motion according to [7] as:

$$(M_{55} + A_{55})\ddot{\beta}_P + B_{55}\dot{\beta}_P + C_{55}\beta_P = F_aL_T, \tag{7}$$

where β_P is the platform-pitch displacement, $\dot{\beta}_P$ is the velocity, $\ddot{\beta}_P$ is the acceleration, M_{55} is the total structural moment of inertia (platform, rotor and tower together are regarded as one rigid-body), A_{55} is the added inertia (from added mass), B_{55} is the radiation damping and linearized viscous damping, C_{55} is the linearized pitch restoring stiffness from hydrostatics and mooring lines, F_a is the aerodynamic thrust and L_T is the hub height. The product of the thrust force and the hub height will act as a torque in the pitch mode of the platform. For small pitch angles, the platform pitch angle can be presented with the translational displacement x_T and the height of the hub L_T as $\beta_P = x_T/L_T$, the equation of motion in pitch mode can consequently be written as:

$$\left(\frac{M_{55}+A_{55}}{L_T^2}\right)\ddot{x}_T + \frac{B_{55}}{L_T^2}\dot{x}_T + \frac{C_{55}}{L_T^2}x_T = F_a. \quad (8)$$

At a steady state above the rated wind speed, a disturbance in hub displacement (tower motion leads to the change in effective wind speed) causes the change of the aerodynamic thrust:

$$F_a = F_{a,0} - \frac{\partial F_a}{\partial V}\dot{x}_T. \quad (9)$$

So the equation (8) of 1-DOF motion in platform-pitch mode can be described as:

$$\left(\frac{M_{55}+A_{55}}{L_T^2}\right)\ddot{x}_T + (\frac{B_{55}}{L_T^2} + \frac{\partial F_a}{\partial V})\dot{x}_T + \frac{C_{55}}{L_T^2}x_T = F_{a,0}, \quad (10)$$

which is a typical second-order system with damping ratio:

$$\zeta = \frac{(B_{55}+\frac{\partial F_a}{\partial V}L_T^2)}{2\sqrt{C_{55}\cdot(M_{55}+A_{55})}}. \quad (11)$$

For land-based wind turbines, the pitch action is relatively slow when compared to the change of the wind speed caused by the tower top motion. The thrust coefficient c_T can therefore be regarded as constant when the wind speed changes. The increase in wind speed will result in an increase in thrust, which means it is positively damped, hence the thrust sensitivity $\partial F_a/\partial V$ contributes as a positive part. That is why the instability problem caused by the negative damping is not significant for land-based wind turbines. However, the first tower natural frequency of the FOWT decreases significantly. With a land-based blade-pitch controller, the action of pitching is faster. c_T is reduced by the increase of the blade pitch and the decrease of the tip speed ratio, which consequently reduces the thrust, so the thrust sensitivity $\partial F_a/\partial V$ will reduce the total damping of the dynamic system, which can consequently lead to a negative damping in platform-pitch mode. As a conclusion, if $\partial F_a/\partial V$ is kept above a reasonable minimum limit, this instability problem can be solved. Qualitatively speaking, the controller should react slower, which can be achieved by reducing the proportional gains of the controller.

3.3. Gain scheduling

Since the aerodynamic torque doesn't follow the Froude scaling, a scaling of the controller parameters from the full-scale turbine is not possible. The controller tuning is re-done for the scaled model and is based on the analysis of simulations results. Different gain scheduling methodologies are developed using linearized versions of the simulation models. The control design followed the procedure of de-rating the proportional gain in order to limit the bandwidth of the controller. With the goal of analyzing this "negative damping" effect in the experiment, the bandwidth was varied for different controllers by tuning the proportional gains.

For land-based wind turbines, the gains are usually scheduled such that a constant drivetrain closed-loop natural frequency ω_Ω and damping ratio ζ_Ω are maintained, see Equation (6). For offshore wind turbines, because of the negative aerodynamic damping, which was introduced in Section 3.2, [6] has suggested that this natural frequency ω_Ω should be lower than the platform-pitch natural frequency to ensure the platform remains positively damped. Hence, several controllers with different gains are investigated (i.e. with different closed-loop natural frequencies). As is presented in Figure 6 (a), the drivetrain closed-loop natural frequency of the controllers C1, C2, C3, are 0.7, 0.9 and 1.1 times the platform-pitch natural frequency, respectively. The damping ratio is kept constant at $\zeta_\Omega = 0.7$. Since the pitch sensitivity $\partial M_a/\partial\theta$ changes over steady state, the gains also change over the steady state to ensure a constant dynamic behavior of the closed-loop as Figure 6 (b) shows, where the corresponding blade-pitch angles represent the steady states.

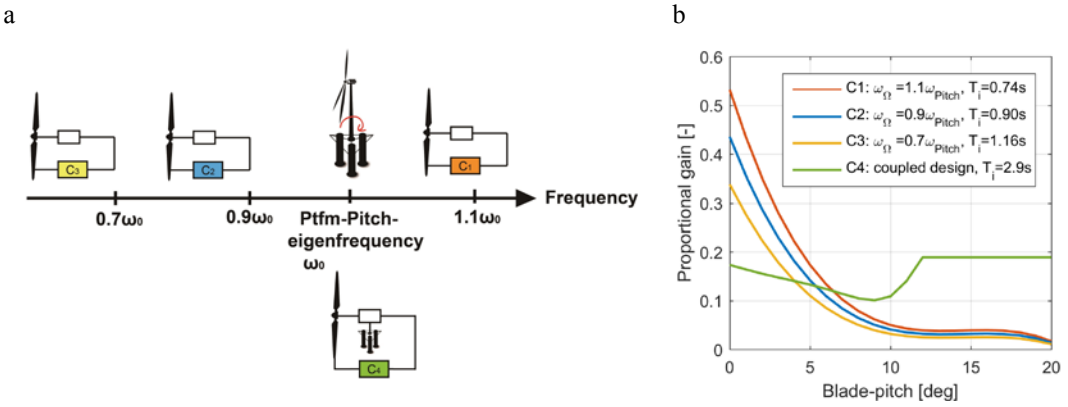

Figure 6: Overview of test controllers with different gains; (b) Proportional gains over blade-pitch angles in steady states.

Another methodology, the "coupled" gain-scheduling methodology is discussed in [8]. Instead of considering the isolated drivetrain closed-loop, the motion of the whole FOWT is taken into account. The FOWT system is regarded as a rigid multibody system with 5 DOFs and set up in a simplified model with linear wave excitations and a quasi-static mooring model. The aerodynamics including the blade-pitch controller are linearized at different wind speeds, with which it is feasible to get the pole-zero plot and determine the stability of the coupled system. The principle idea of the coupled gains is to keep the real part of the pole in pitch mode constant for each wind speed and find the corresponding proportional gain K_P.

For C4, the poles at wind speed 1.6 m/s with K_P varying from 0.1 to 0.4 and different time constants T_i are plotted in Figure 7 (a), in which the influence of K_P and T_i on the stability of the pitch mode is indicated. First, some of the poles with larger K_P, have a positive real part, which means the platform-pitch mode is not stable. Second, an increased T_i tends to make this mode more stable, however improvement of the stability is limited. Especially for T_i greater than 2.9 s, the position of the poles doesn't change so much to bring a remarkable improvement on the platform-pitch mode stability. Thus, $T_i = 2.9$ s is chosen, with which the poles at different wind speeds, i.e. steady states are analyzed as Figure 7 (b) shows. It is clear that the influence of the proportional gain K_P on the pitch mode's stability differs for different wind speeds. At higher wind speeds, the negative aerodynamic damping has much less influence. For example, when $V_0 = 1.9$ m/s, if the real part of the pole $R(\lambda)$ is limited within $-5 \cdot 10^{-2}$ (marked with red dashed-line in Figure 7 (b)), the restriction on K_P is not strict, since all the gains satisfy the stability requirement. By interpolating within proportional gains and wind speeds, the gains with placed poles can be calculated, which are plotted in Figure 6 (b). To simplify the hardware implementation, K_P is a polynomial function for smaller blade-pitch but kept constant when the blade-pitch is greater than 12 deg.

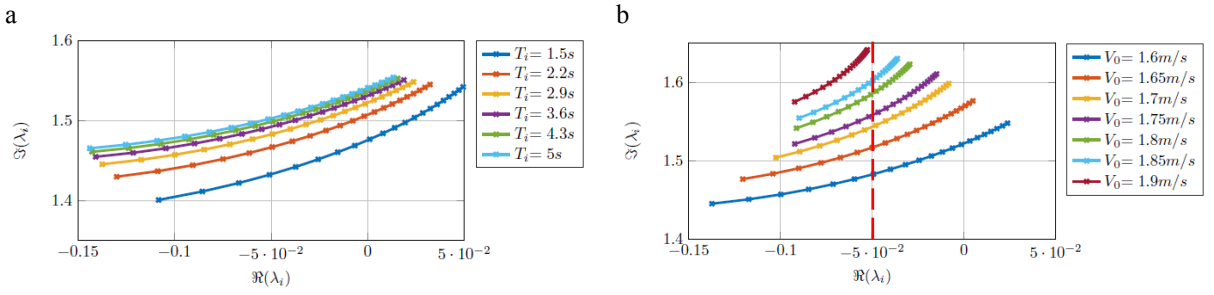

Figure 7: Poles in pitch mode with K_P=0.1…0.4 at wind speed 1.6 m/s (a) and T_i=2.9 s (b).

4. Hardware implementation of the controller

The designed controllers are implemented on an Arduino board. Detailed implementation is presented in this section, including the hardware setup, the signal acquisition and the determination of the loop frequency.

4.1. Hardware setup of the control loop

Figure 8 shows the final hardware setup of the control loop, including two JVL MAC050 integrated servomotors, microcontroller, an Ethernet-shield, a router and a power supply. The two servomotors act as the torque- and the blade-pitch- actuator, respectively, which are equipped with the EM4 expansion module and able to communicate with the industrial standardized Modbus protocol over TCP/IP.

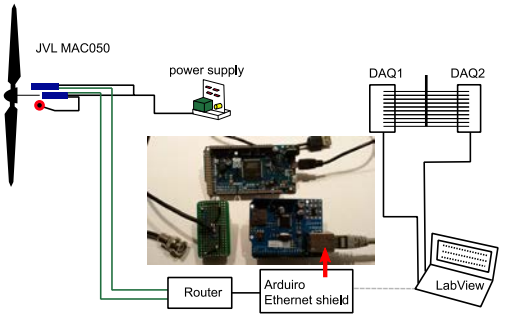

Figure 8: Hardware setup of the control loop.

The Arduino-Due board is used as a microcontroller because of its open-source prototyping platform and affordable price. LabVIEW is used only to log test data both from Arduino and analog-signal data acquisition system at DHI. Embedded Coder by Matlab is used to generate the C++ code for each step of the control loop. This generated one-step code is associated with a real-time clock and executed in Arduino. Signals for the controller are acquired by the serial communications protocol Modbus, which is based on a master and slave architecture. In the test, the Arduino works as a master which transmits requests (blade-pitch angle or motor torque) to the slave (servomotors).

4.2. Signal acquisition

Initial tests on signal acquisition of the servomotors are performed by accelerating the servomotor stepwise from 0 rpm to 1700 rpm. The measured motor speed from the speed register shows large fluctuations, and even “jumps” as Figure 9 (a) shows, with an approximate standard deviation of 65 rpm.

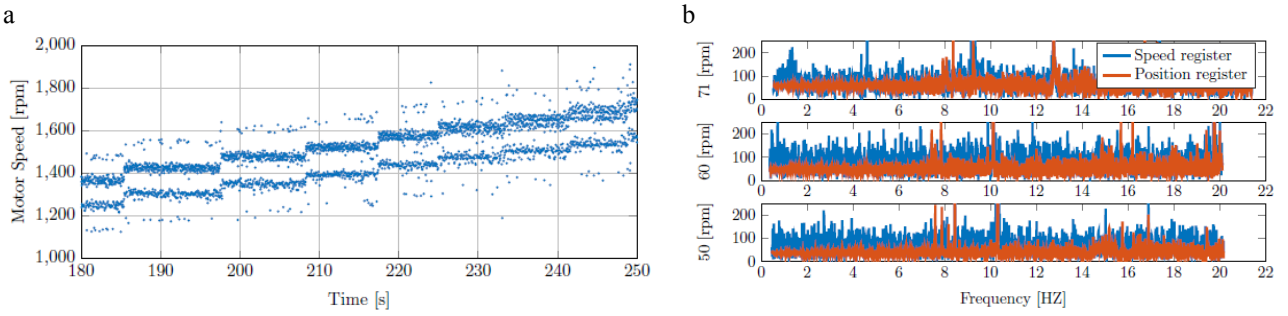

Figure 9: (a) Measured speed with speed register; (b) Comparison of measured speed in frequency domain with different register.

The problem discovered on this issue is that the measurement resolution of the speed register is approximately 8 rpm, which ultimately involves a quantisation noise amounting to $\pm$ 8 rpm [10]. Since the position register has a 32 bit data format (motor speed register only 16 bit) and its unit is encoder counts (encoder sampling frequency is 520.8Hz), it was decided to get the motor speed by differentiating the motor's current position instead of requiring data from the speed register, which is calculated as:

$$\Omega = -\frac{\varphi_{\mathrm{Loop}_n} - \varphi_{Loop_{n-1}}}{\delta T_{Loop}}, \tag{12}$$

where φ is the real-time motor position and δT_{Loop} is the exact time interval between two loops. The time which is needed for requesting register data varies by up to 2 ms and therefore time stamps are used to calculate the time interval δ_{Loop}.

A low-pass filter is implemented to smooth out high frequencies. Regarding the existing system, a discretized first order filter is used, which can be derived by discretizing the Laplace transfer function. A common discretization method in control applications is the (Euler) Backward differentiation method, which is:

$$\Omega_f(t_n) = \frac{T}{T+\delta t}\Omega_f(t_{n-1}) + \frac{\delta t}{T+\delta t}\Omega(t_n) \tag{13}$$

The filter is a first order low-pass filter. According to Equation (13), the present filter output $\Omega_{\mathrm{f}}(\mathrm{t_n})$ is a function of the present filter input $\Omega(\mathrm{t_n})$ and the filter output at the previous discrete time, $\Omega_{\mathrm{f}}(\mathrm{t_{n-1}})$. The filter output is stored in Arduino so that it is available for the filter algorithm at the following execution. Regarding the filtering in the test: At the low-speed shaft the 1p-frequency is equal to 1.17 Hz for rated. The final cut-off frequency is chosen as 7 Hz.

4.3. Loop frequency

The communication between the Arduino and the servomotors via Modbus in each loop turned out to be time-consuming, which results in a maximum 45 Hz loop frequency. At the end of each loop, a wait function is applied to delay the execution of the next loop, which ensures a constant loop time. However, since the time gap between the end of one execution of the loop and the start of the next execution requires a few clock cycles, which means that the action of measuring how long it takes affects how long it takes, the real-time clock is not exactly in real-time, in other words, the loop time is not kept exactly constant.

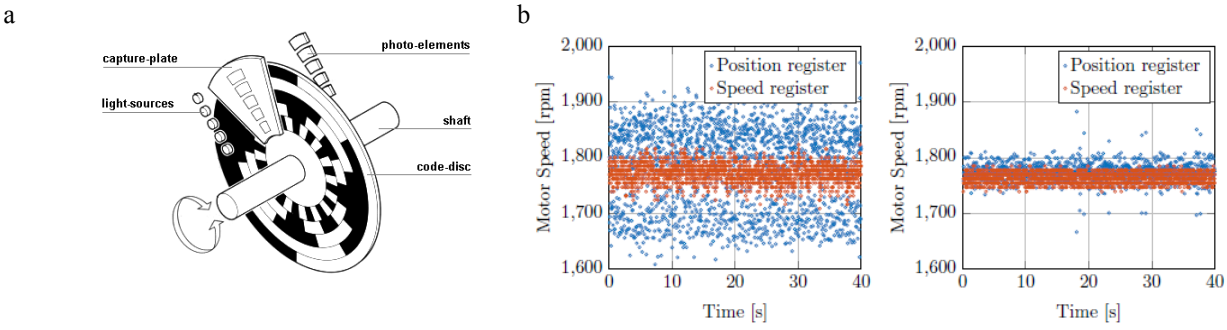

Figure 10: (a) Encoder mechanism [11]; (b) Comparison of measured speed with before (left)- and after (right)-changing loop frequency.

The signal measurement frequency was designed to be the same as the loop frequency (45Hz), which means the δT_{Loop} in (12) is $1/45$ s. It is over 11 times slower than the sampling frequency of the encoder (520.8Hz). For this reason a large measurement error is discovered (see Figure 10 (b)), since the quotient of the encoder sampling frequency and signal measurement frequency $520.8\mathrm{Hz}/45\mathrm{Hz} = 11.57$ is a floating point number. Figure 10 (a) illustrates a simple rotational absolute encoder. The number of light-sources n decides how accurate this encoder's sampling is according to the number of distinct positions of the shaft (2^n). For example, the JVL has 12 light-sources, so there are 2^{12} positions and the resolution should be $360/4096 = 0.0879$ deg. These light-sources count 520.8 times per second to track the unique positions to record the motor's rotational position. However, Modbus request the

data of position 45 times per second. That means, sometimes Modbus requests register data in the middle of the counting by light-source, so that it gets the information after the light-sources' 11 counts, or gets data after 12 counts, there is always a position difference even when the motor has a constant speed. Taking this into consideration, the signal acquisition frequency is increased to 40 Hz, which makes the ratio an integer, i.e. $520.8\text{Hz}/40\text{Hz} = 12$. The improvement is quite remarkable, which can be derived from Figure 10 (b) with the sampling rate 40Hz on the right.

5. Wave tank tests and results

Tests under a wide range of sea states and wind speeds were carried out throughout the test campaign. Some results relating to the controller will be presented and discussed below. The environmental conditions for the load case (LC) discussed in this section are given in Table 1.

Table 1: Load cases for the tests.

Load case	Model scale			Full scale		
	H_s [m]	T_p [s]	V [m/s]	H_s [m]	T_p [s]	V [m/s]
1	0.091	1.08	1.89	5.46	8.37	14.64
2	0.159	1.43	1.89	9.54	11.1	14.64

5.1. Discussion of the test results

The comparison of the response between fixed blade-pitch test and pitch-control test in LC2 is shown in Figure 11 (regular wave) and Figure 12 (irregular wave), where Ω is the rotor speed, θ is the blade-pitch angle, M_g is the servomotor torque, β_P is the platform-pitch rotational displacement and H_s represents the significant wave height. Plots on the left side are in time domain and those on the right side are in frequency domain. It should be mentioned that "pitch-fixed" in the plot means that the blade-pitch and rotor speed are both preset and constant for each test and "pitch-control" implies that the rotor speed is controlled with the controller C4 designed in Section 3.3. Obviously, the rotor speed is kept below 110% of the rated rotor speed (71 rpm), which proves that a controller design procedure with a simplified low-order simulation model is effective.

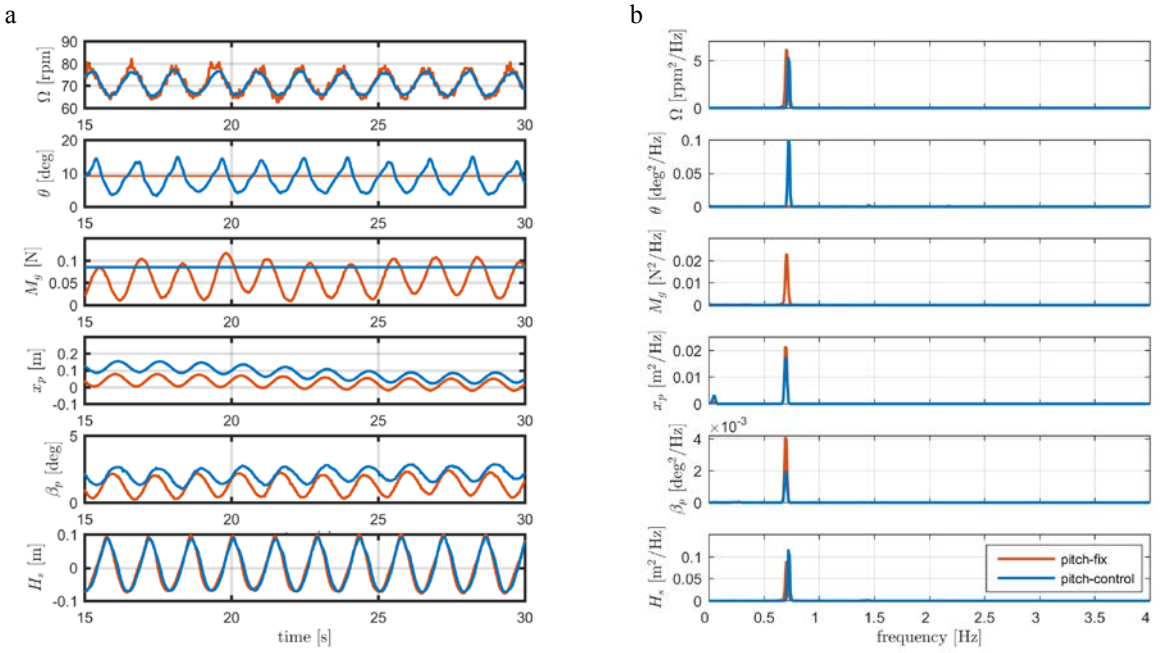

Figure 11: (a) Regular wave response in time domain (LC2); (b) Regular wave response in frequency domain (LC2).

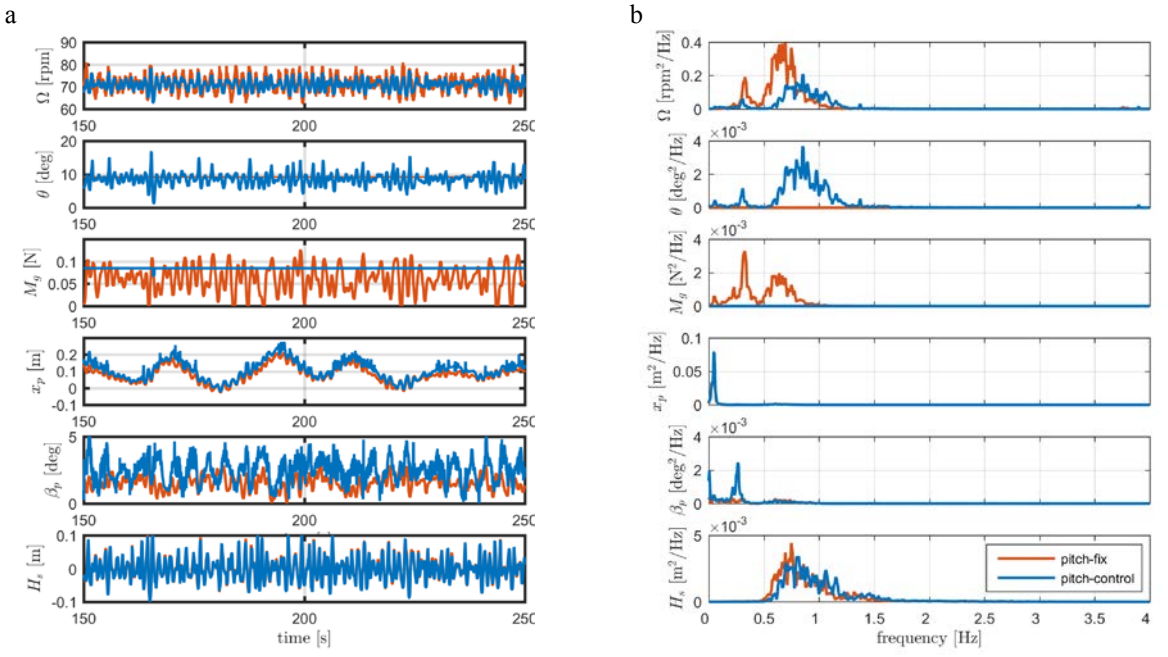

Figure 12: (a) Irregular wave response in time domain (LC2); (b) Irregular wave response in frequency domain (LC2).

A problem discovered in Figure 11 (a) is that the rotor speed in the pitch-fix test is not fixed as expected, as is evident from the sinusoidal signal of the rotor speed Ω. The reason for this is that the fixed rotor speed is achieved by a servomotor. The servomotor keeps a constant rotational speed as long as the resultant torque acting on the shaft is zero, which means the aerodynamic torque from one side and the motor torque from the other side should be in

equilibrium. This equilibrium is achieved by adjusting the motor torque through an internal PID-controller in the servomotor. Since the aerodynamic torque changes with the relative wind speed, which is influenced by the wind, wave and the movement of the platform, the motor torque needs to be regulated according to the change of aerodynamic torque. As a consequence, the rotor speed can only be kept quasi constant. Regarding the unfixed rotor speed in control group, some conclusions can be drawn. First, rotor speed control above the rated wind speed with torque regulation has much lower motion response in the platform-pitch mode, which can be explained by the disappearance of negative aerodynamic damping, since the blade-pitch is kept constant. Meanwhile, the rotor speed in the pitch-control test has less fluctuation, which shows that control with blade-pitch is more effective than with torque.

The power spectral density (PSD) of the response in irregular wave (LC1) is presented in Figure 13. The performance of the four controllers, which are introduced in Section 3.3, is compared in frequency domain. The design of C1, C2 and C3 uses a 1-DOF model and C4 is designed with a coupled 5-DOF model. Identified resonance frequencies corresponding to the modes of the platform-pitch, wave and rotor speed 3P are marked respectively.

In the platform-pitch mode, the wind and wave induced response with controller C1 is the greatest. Response with controller C2 is smaller than that with C1, but still much greater than C3. This result agrees well with the expectation which is explained in Section 3. When the controller is so fast that the natural frequency of the drivetrain closed-loop exceeds the natural frequency of the platform-pitch, the instability problem due to the negative aerodynamic damping will probably appear. Thus, reducing the bandwidth of the controller (or make the controller slower) can mitigate the instability problem in platform-pitch mode. However, this method doesn't reduce the response within the range of wave frequencies, as evidenced by the similar amplitude in platform-pitch mode.

Another issue that can be observed is that detuning the gains changes the system dynamic properties significantly. As can be seen, the resonance frequencies in the rotor speed, blade-pitch and platform-surge modes are changed. It should also be mentioned that reducing the bandwidth comes at the cost of the control performance. About the controller C4 which is a coupled design, has less wave-induced response in comparison to the other three with detuned gains.

In conclusion, detuning based on the principles of a land-based controller is insufficient; a more conservative controller (i.e. smaller gains) changes the coupled natural frequencies more. Otherwise, it leads to the instability problem with greater gains.

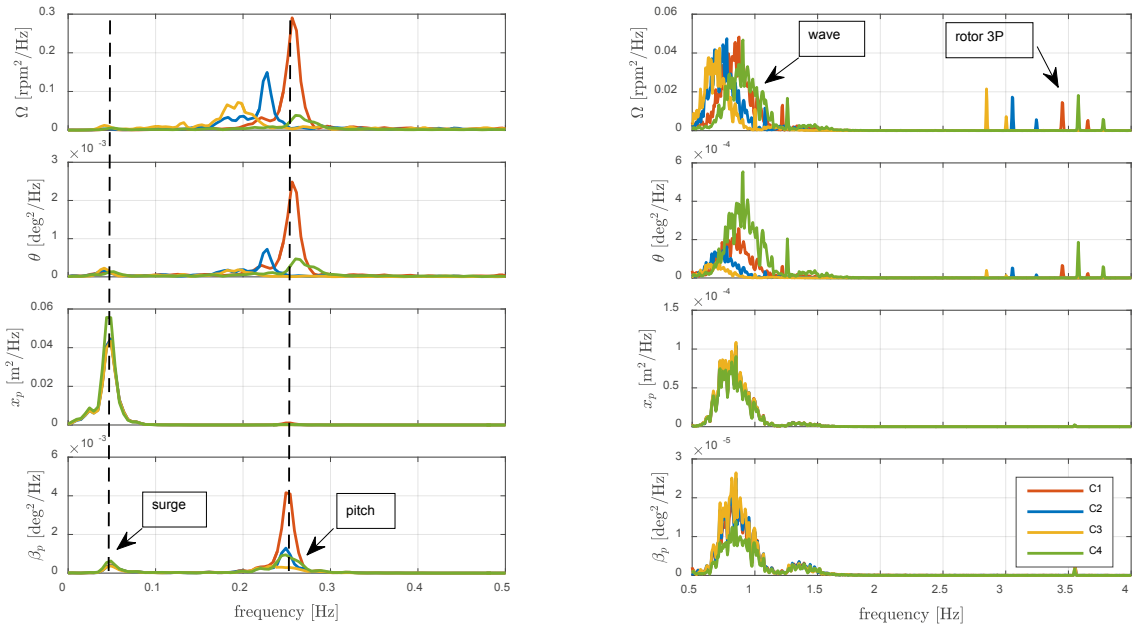

Figure 13: Response in frequency domain with 4 different blade-pitch controllers in irregular wave (LC1).

5.2. Validation of simulation model

Simulation models of FOWTs are validated normally with fixed blade-pitch tests [1]. The underlying problem is the question whether such a validated simulation model can also reproduce the motions and loads with a controller at the same level; in other words, whether simulations coupling the servo dynamic require a higher fidelity model. Figure 14 shows the comparison of the validation between the reduced simulation model and the test model in regular waves (LC2).

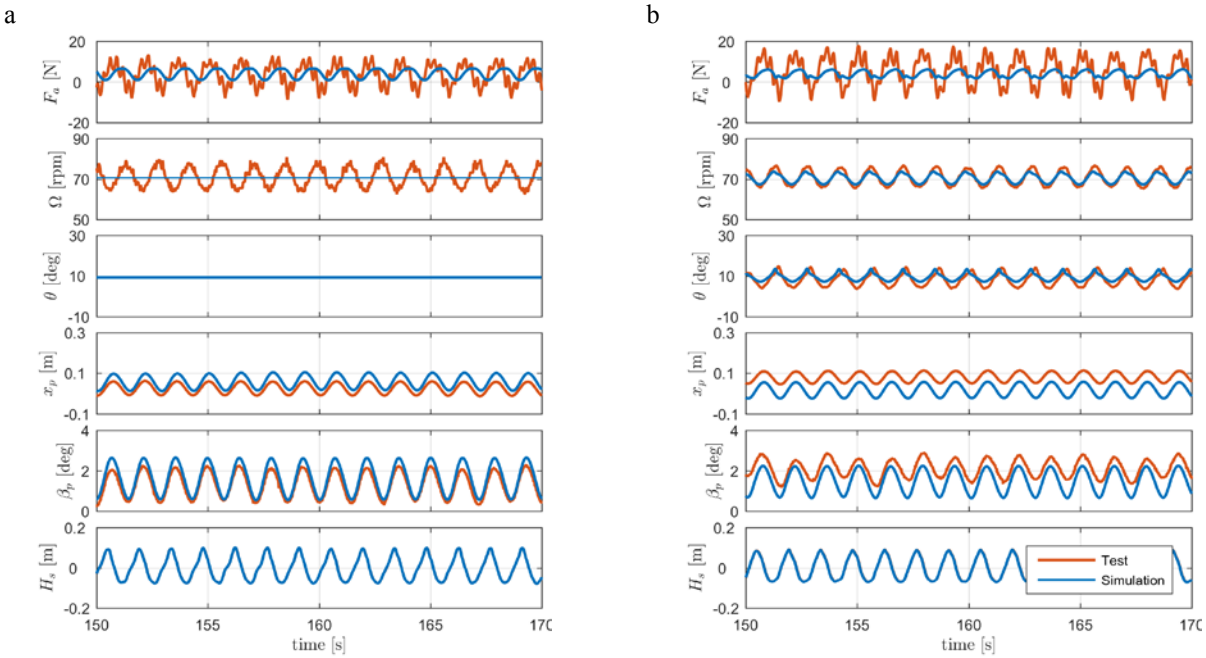

Figure 14: (a) Validation with blade-pitch fixed test in regular wave (LC2); (b) Validation with blade-pitch control in regular wave (LC2).

The test with a fixed blade-pitch angle shows a satisfactory agreement in terms of platform motion. A small disagreement on amplitude is discovered, likely because the motion-dependent hydrodynamic damping was simplified as a linear damping, which is determined through a pitch decay test, in which the platform motion frequency is much lower. The offset of the platform-surge may come from the uncertainty of the anchor position during the test. The reason for the large misalignment on the thrust is that the rotor speed is not exactly constant but changes sinusoidally, which is missing in the simulation model.

Concerning the validation with the controller which is shown in Figure 14 (b), it can be seen that all the disagreements are enlarged, i.e. the aerodynamic thrust and the motion of the platform. The amplitude of the thrust with blade-pitch control in the test is much greater than the one in simulation. This can be explained by the sensitivity of the thrust coefficient c_T. In the pitch-fixed test, the change of thrust comes only from the tip speed ratio and hence the aerodynamic behavior is less influenced since c_T is less sensitive to the tip speed ratio. However, with the blade-pitch control, more uncertainty is included in the simulation model: e.g. for the pitch actuator system, the time-delay of the control system and the measurement error of the rotor speed et cetera. These factors can lead to a greater error by predicting the aerodynamics. Thus, validation of simulation models with control system is more complicated. There is also less reliability if the simulation model is validated without control system.

Another issue that will be discussed is whether a high fidelity model is necessary to design the control system for FOWTs. It has been shown previously that a model with only one single drivetrain DOF is not sufficient, but it remains to be answered how well the simplified low-order model with 5-DOFs matches the test model, which is effective for the controller design. An extra comparison of wind and irregular wave induced response in both LC1 and LC2 is presented in Figure 15. The resonance frequencies including surge, pitch and the range of wave frequencies agree

well, which means that natural frequencies of different modes of the dynamic system can be predicted by the simplified model. In the range of wave frequencies, the response in the platform-surge and -pitch modes agree well, whereas there is a slight difference regarding the blade-pitch and rotor speed modes, which is believably due to the time delay and the relatively lower loop frequency of the controller introduced in Section 4.3. In the lower frequency region, in both of the load cases, a great difference between the test and the simulation exists due to the lack of second order wave excitation. In the higher frequency region, results in LC2 matches better. It should be mentioned that the motion capture sensors didn't work well in LC2 because some balls for camera tracking got wet, which affected the reflection. As a consequence, response in surge x_P and pitch β_P of LC2 are quite different (for example, they don't have the rotor 3P excitation). The rotor speed 3P excitation isn't replicated in simulation model since the rotor is modelled as an actuator disk.

To summarise, the simulation model cannot predict the motions well due to the many simplifications. However, the controller C4 which is designed through this simplified model showed good performance in controlling the rotor speed.

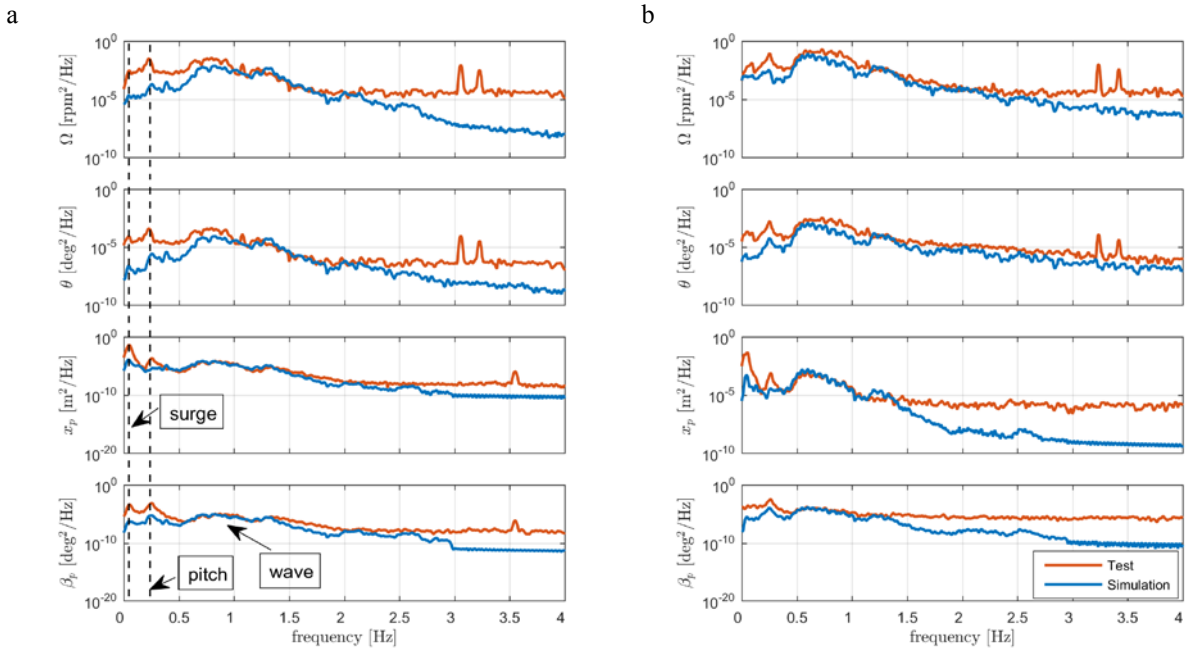

Figure 15: (a) Response in irregular wave (LC1); (b) Response in irregular wave (LC2).

6. Conclusion

This paper is a partial presentation of the Triple Spar Campaign with an objective of investigating the wind- and wave-induced response of a scaled real-time controlled FOWT. Tests under a series of wind-wave combined load cases are carried out at the wave tank of DHI in Hørsholm, Denmark. Some difficulties are discovered from the hardware implementation. Measurement of rotor speed with higher resolution and precision is recommended, as well as an accurate clock to execute control loops. The low resolution of the Arduino with Modbus communication via TCP/IP seems not sufficient, because nonlinear behavior of the blade pitch and rotor speed is discovered in regular waves. The reduced simulation model can't reproduce the response outside the wave frequency region well, however is efficient and functional for controller design. It has been shown that the dynamic behavior of the FOWT with a controller is different from the blade-pitch fixed tests, which has been more commonly used in the past. Thus, it is recommended that wind-wave combined model tests should be performed with active control.

Acknowledgements

This research was financially supported by University of Stuttgart, Technical University of Denmark and National Renewable Energy Centre of Spain. We would also thank Maayen Wigger for helping with the Modbus communication and Florian Amann for building the platform model.

References

[1] K. Müller, F. Sandner, H. Bredmose, J. M. A. Azcona and R. Pereira, "Improved Tank Test Procedures For Scaled Floating Offshore Wind Turbines," in *International Wind Engineering Conference IWEC*, Bremerhaven, 2014.

[2] J. Azcona, F. Bouchotrouch, M. González, J. Garciandía, X. Munduate, F. Kelberlau und T. A. Nygaard, Aerodynamic Thrust Modelling in Wave Tank Tests of Offshore Floating Wind Turbines Using a Ducted, Journal of Physics: Conference Series, Volume 524, conference 1, 2014.

[3] R. F. Mikkelsen, "The DTU 10MW 1:60 model scale wind turbine blade," 2015.

[4] F. Amann and F. Lemmer, "Design Solutions for 10MW Floating Offshore Wind Turbines," *INNWIND.EU, Deliverable D4.37,* 2016.

[5] H. Bredmose, F. Lemmer, M. Borga, A. Pegalajar-Juradoa, R. Mikkelsena, T. F. T.Stoklund Larsena, W. Yu, A. Lomholta, L. Boehma and J. A. Armendariz, "The Triple Spar campaign: Model tests of a 10MW floating wind turbine with waves, wind and pitch control".

[6] T. J. Larsen and T. D. Hanson, "A method to avoid negative damped low frequent tower vibrations for a floating, pitch controlled wind turbine," *Journal of Physics: Conference Series,* vol. 75, p. 012073, 2007.

[7] J. M. Jonkman, *Influence of Control on the Pitch Damping of a Floating Wind Turbine,* Reston, Va.: American Institute of Aeronautics and Astronautics, 2008.

[8] F. Sandner, D. Schlipf, D. Matha and P. W. Cheng, "Integrated optimization of floating wind turbine systems," in *Proceedings of the 33rd International Conference on Ocean, Offshore and Arctic Engineering OMAE, San Francisco, USA*, 2014.

[9] J. M. Jonkman, Dynamics modeling and loads analysis of an offshore floating wind turbine, ProQuest, 2007.

[10] A. JVL Industri Elektronik, "Integrated Servo Motors Technical Manual," 2005.

[11] J. Weidemann, *Instrumentation: How does an encoder work?,* 2012.